Journal of Molecular Structure 1359 (2026) 145427

Contents lists available at ScienceDirect

Journal of Molecular Structure

journal homepage: www.elsevier.com/locate/molstr

Cu^{II} complexes with *N*-(5-(methylthio)-1,3,4-thiadiazol-2-yl)benzamides: Synthesis, characterization and biological evaluation

Ana Júlia Zimmermann Londero [a], Ulrich Abram [b], Maximilian Roca Jungfer [c], Gabriela Nanci Ledesma [d], Jennyfer Castro [e], Camilla Abbehausen [e], Vânia Denise Schwade [a,*]

[a] Department of Chemistry, Natural and Exact Sciences Centre, Federal University of Santa Maria, Av. Roraima, 1000, 97105-900 Santa Maria, RS, Brazil
[b] Institute of Chemistry and Biochemistry, Freie Universität Berlin, D-14195 Berlin, Germany
[c] Institut fuer Nukleare Entsorgung, Karlsruher Institut fuer Technologie, D-76344 Eggenstein-Leopoldshafen, Germany
[d] Instituto de Química Rosario (IQUIR), Consejo Nacional de Investigaciones Científicas y Técnicas, Facultad de Ciencias Bioquímicas y Farmacéuticas, Universidad Nacional de Rosario, Suipacha 531, S2002LRK Rosario, Argentina
[e] Institute of Chemistry, University of Campinas, Rua Monteiro Lobato, 270, 13083-862 Campinas, SP, Brazil

ARTICLE INFO

Keywords:
Cu^{II} complexes
1,3,4-thiadiazole moiety
Fluorinated benzamides
Anticancer activity

ABSTRACT

4-Fluoro-*N*-(5-(methylthio)-1,3,4-thiadiazol-2-yl)benzamide (HL^1) and 2,3,4,5,6-pentafluoro-*N*-(5-(methylthio)-1,3,4-thiadiazol-2-yl)benzamide (HL^2) were prepared through reaction with 2-amino-5-(methylthio)-1,3,4-thiadiazole and the corresponding aroyl chlorides. They have a planar *cis*-orientation concerning the carboxamide oxygen atom and the thiadiazole sulfur atom. The short intramolecular S•••O contact upon the *cis*-orientation in HL^1 was studied by DFT calculations. The HL molecules are luminescent in the solid-state and solution. The reaction of HL^1 with $CuCl_2$•$2H_2O$ in methanol/dichloromethane mixture produces $[Cu(CH_3OH)_2Cl_2(HL^1)_2]$ (**1**) and $[Cu(L^1)_2]$ (**2**). Compound **2** is formed when NEt_3 is used, or the used copper salt is replaced by $Cu(Ac)_2$•H_2O. Given the low solubility of compound **2**, a reaction of HL^2 with $CuCl_2$•$2H_2O$ was performed in methanol with the addition of NEt_3 as supporting base, yielding $[Cu(L^2)_2]$ (**3**) and polymorph **3B**. The molecular structures of the products were determined by single-crystal XRD. All compounds were characterized by elemental analysis, FT-IR and UV-Vis/DRS spectroscopies, and ESI mass spectrometry. HL^1, HL^2 and compound **1** were also analyzed by NMR spectroscopy. HL^1, HL^2, and complexes **1** and **3** were evaluated for their cytotoxicity against MCF-7 cells and non-tumorigenic HaCaT cells. Complexes **1** and **3** exhibited cytotoxic activity against MCF-7, with CC_{50} values of 5.02 ± 1.97 μM and 7.88 ± 2.16 μM, respectively, while the ligands HL^1 and HL^2 are non-cytotoxic at the tested concentrations.

1. Introduction

1,3,4-Thiadiazoles are five-membered heterocyclic compounds which have a wide range of applications in the fields of medicinal chemistry, materials science, and agriculture [1]. Applications mostly focus on their charge-transporting capacity, photoluminescence, photoconductivity, mesomorphism to obtain liquid crystals, anticorrosive activity on metal surfaces, etc., [2]. Moreover, their vast pharmacological activitiy [3] continues to motivate researchers for investigation of new compounds containing 1,3,4-thiadiazole substructures.

Neutral 1,3,4-thiadiazoles normally coordinate copper ions through the nitrogen atom(s) of the thiadiazole ring. When both nitrogen atoms coordinate, dinuclear [4] to polymeric [5] compounds are obtained. Molecules containing an amide group [−NHC(O)R] at a carbon position of the 1,3,4-thiadiazole ring can act as anionic ligands, coordinating through nitrogen and oxygen atoms forming *N,O*-chelates. To the best of our knowledge only one example has been reported in the literature (R = Me) until now [6].

In this work, 4-fluoro-*N*-(5-(methylthio)-1,3,4-thiadiazol-2-yl)benzamide (HL^1) and 2,3,4,5,6-pentafluoro-*N*-(5-(methylthio)-1,3,4-thiadiazol-2-yl)benzamide (HL^2) (Fig. 1b) were prepared and fully characterized. The adopted structural conformations are discussed based on experimental single crystal X-ray crystallography and

* Corresponding author.
E-mail address: vania.schwade@ufsm.br (V.D. Schwade).

https://doi.org/10.1016/j.molstruc.2026.145427
Received 12 November 2025; Received in revised form 30 December 2025; Accepted 19 January 2026
Available online 21 January 2026

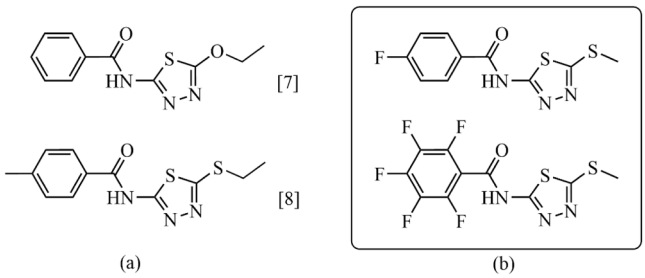

Fig. 1. Structural formulae of (a) representative molecules containing alkoxy or thioxy groups [7,8]. Both have been structurally analyzed by SC-XRD; (b) the HL molecules as ligands in this work.

spectroscopic data, and complemented by density functional theory (DFT) calculations. The potentially stabilizing effect of an often-claimed S•••O interaction in the molecular arrangement of such ligands was studied. Three mononuclear copper(II) complexes were obtained: [Cu$(CH_3OH)_2Cl_2(HL^1)_2$] (**1**), [Cu$(L^1)_2$] (**2**), and [Cu$(L^2)_2$] (**3**). The effects of HL^1, HL^2, and complexes **1** and **3** on cell viability were evaluated using estrogen receptor-positive human breast adenocarcinoma cell line (MCF-7), and, an immortalized, non-tumorigenic human keratinocyte cell line (HaCaT) frequently used as a model of normal cells.

2. Results and discussion

Preparation and structural description of 4-fluoro-*N*-(5-(methylthio)-1,3,4-thiadiazol-2-yl)benzamide (HL^1) and 2,3,4,5,6-pentafluoro-*N*-(5-(methylthio)-1,3,4-thiadiazol-2-yl)benzamide (HL^2)

The ligands HL^1 and HL^2 were prepared by reacting the corresponding benzoyl chlorides with 2-amino-5-(methylthio)-1,3,4-thiadiazole in dry THF and with NEt_3 as a supporting base following the protocol described by Cho *et al.* [8], recently applied to a diamide type ligand [9]. Purification of the crude products by recrystallization from CH_2Cl_2/MeOH afforded HL^1 and HL^2 in good yields (90 and 71%, respectively). Both compounds displayed good solubility in several solvents, including *N,N*-dimethylformamide, dimethyl sulfoxide, acetonitrile, dichloromethane, and dichloromethane/methanol mixture.

Single crystals of HL^1 and HL^2 suitable for X-ray diffraction were grown from CH_2Cl_2/MeOH. Crystal data and details of structure refinement are detailed in Table S1 (HL^1) and Table S2 (HL^2). The asymmetric unit comprise one HL^1 molecule, while four independent molecules of HL^2 (Figs. S1 and S2). The molecules are planar, although the acetylamino group is slightly twisted from the plane of the 5-(methylthio)-thiadiazole ring with torsion angle of 2.44(1)° for HL^1 (Table S5). The torsion angles for HL^2 range from −0.9(3) to 2.2(3) Å. The amide C=O and C−N bond lengths in HL^1 [1.221(2) and 1.379(2) Å, respectively] and HL^2 [1.213(2)-1.216(2) and 1.351(2)-1.360(2) Å, respectively] (Table S4), are close to the bond lengths in the related molecules depicted in Fig. 1a (1.22 and 1.37 Å, respectively) [7,8]. The molecules are packed in dimeric units bonded by two intermolecular N-H•••N hydrogen bonds (Fig. 2, Fig. S7, Table S3). A pair of intermolecular N-H···N hydrogen bonds links molecules through an inversion center, a feature also observed in the crystal structure of similar molecules [7,8].

The spatial arrangement of the amide oxygen atom and the thiadiazole sulfur atom in the HL^1 and HL^2 molecules suggests an O•••S intramolecular interaction. In HL^1, the O1•••S1 distance is 2.5418(4) Å, while in HL^2 the related O•••S distances are in the range of 2.688(2)-2.731(2) Å (Table S5). For both compounds, the distances are shorter than the sum of the van der Waals radii of the S and O atoms (3.35 Å [10]). The potential for such interaction or even chalcogen bond has been evaluated by DFT methods through analyses based on the topological interpretation of the electron density using a quantum theory of atoms in molecules (QTAIM) approach (see related section below).

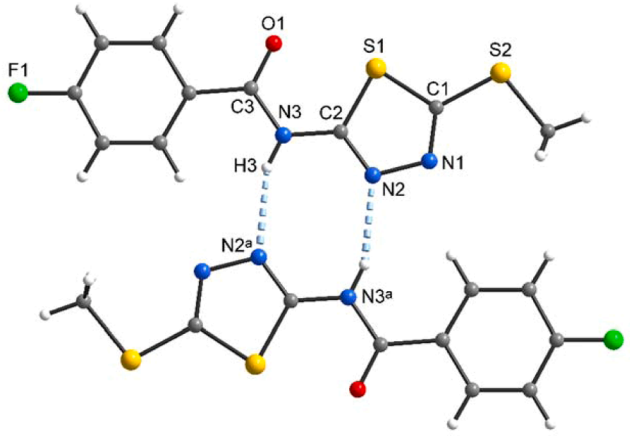

Fig. 2. Molecular structure of HL^1. The molecules interact producing dimers. Symmetry operator: [a] $-x+2, -y+1, -z+1$. Hydrogen bonds are shown in light blue dashed lines.

2.1. HL^1 and HL^2 NMR and FTIR data

NMR spectra were collected for HL^1 and HL^2 in DMSO-d_6 (see Figs. S12-S14, and Figs. S18-S20 for ^{1}H, ^{13}C and ^{19}F spectra of HL^1 and HL^2, respectively). For HL^1, the signals of the carbon atoms of the 1,3,4-thiadiazole ring are found at 159.3 (carbon atom bonded to the amide group) and 160.7 ppm (carbon atom bonded to the methylthio group). For HL^2, the related signals of the carbon atoms were found at 156.3 and 162.0 ppm. For 5-ethylthio-2-*p*-toluoylamimo-1,3,4-thiadiazole, the signals of the corresponding carbon atoms were observed at 161.3 and 160.1 ppm in $CDCl_3$ [8]. The carbon atom from the C-F bond in HL^1 was observed as a doublet at 164.9 ppm ($^1J_{C\text{-}F}$ = 251.4 Hz). In 4-fluoro-benzamide derivatives, doublets at ca. 165 ppm with $^1J_{C\text{-}F}$ of 250.5 and 269.2 Hz have been observed in $CDCl_3$ [11]. In HL^2 spectrum, the three doublets [143.7 ($^1J_{C\text{-}F}$ = 251.0 Hz), 142.4 ($^1J_{C\text{-}F}$ = 255.1 Hz), and 137.2 ($^1J_{C\text{-}F}$ = 251.3 Hz)] confirm the pentafluorobenzamide fragment. An unambiguous structural assignment of the ^{1}H and ^{13}C resonances was confirmed by the 2D NMR spectra (see Figs. S15-S17 for HL^1, and Figs. S21 and S22 for HL^2).

In the FT-IR spectra of HL^1 and HL^2 (Fig. S25 and S26), the ν(N-H) vibration band appeared at 3147 and 3188 cm^{-1}, while the ν(C=O) vibration band of the amide group was observed at 1661 and 1695 cm^{-1}, respectively. Molecules containing similar functional groups exhibit the ν(C=O) band in the 1656-1686 cm^{-1} range [8]. The bands at 1505 (HL^1) and 1496 cm^{-1} (HL^2) can be assigned to the δ(CNH) vibration [12]. The bands at 1432 (HL^1) and 1421 cm^{-1} (HL^2) probably correspond to the C-S stretching vibration of the -SCH_3 group [13] and to the methyl bending (1410 and 1400 cm^{-1}, respectively) [14]. At around 1070 cm^{-1} appears the ν(N–N) vibration [15].

2.2. HL^1 and HL^2 UV-Vis and PL properties

The UV-Vis absorption spectra of HL^1 and HL^2 in DMSO show bands centered at 256 and 299 nm, related to the π−π* and n−π* transitions, respectively (see Fig. S33). The photoluminescence (PL) emission spectra of these molecules in DMSO solution, obtained using fluorescence spectroscopy, are shown in Fig. 3. HL^1 presented an emission band centered at 450-457 nm (λ_{exc} 340-365 nm). HL^2 showed more than two emission bands being the most intense centered at 413 and 435 nm (λ_{exc} 356 nm). The excitation spectra are presented in Figs. S36 and S37. HL^1 has stronger fluorescence compared to HL^2 and was also analyzed by solid-state fluorescence measurements. The emission band at 393 nm presented its higher intensity by excitation at 335 nm (Fig. 4).

Cu^{II} complexes of HL^1 and HL^2: [Cu$(CH_3OH)_2Cl_2(HL^1)_2$] (1), [Cu$(L^1)_2$] (2), and [Cu$(L^2)_2$] (3)

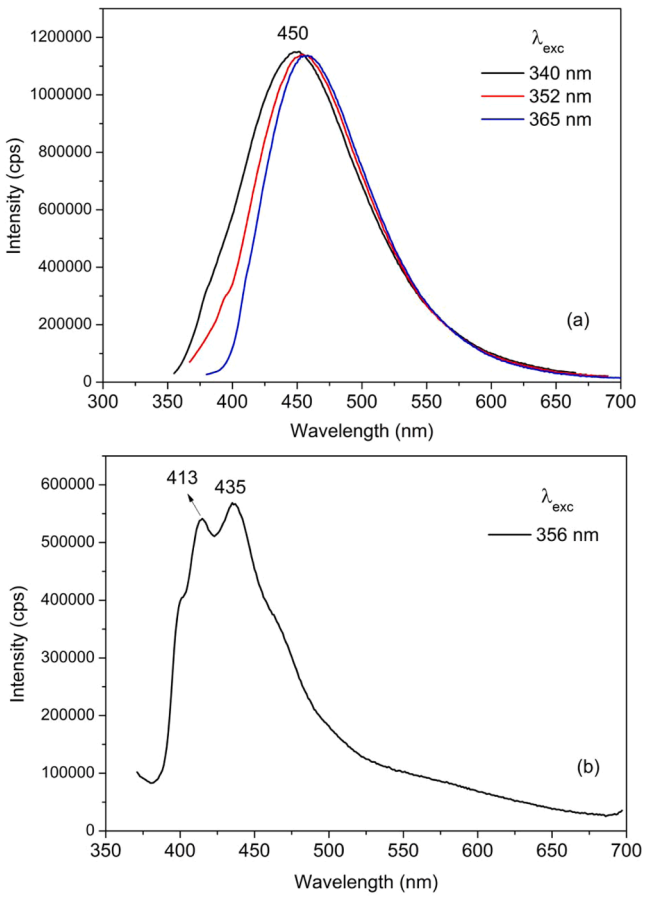

Fig. 3. PL emission spectra of (a) HL^1 and (b) HL^2 in DMSO solutions (5×10^{-4} mol L^{-1}).

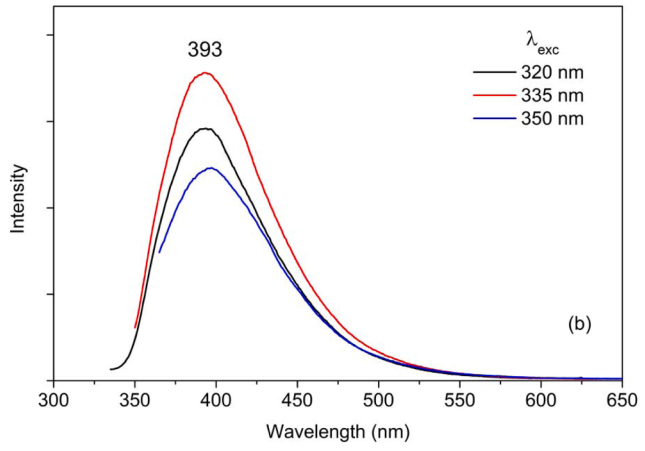

Fig. 4. PL emission spectra of HL^1 in the solid-state.

The reaction of HL^1 with $CuCl_2\bullet2H_2O$ in dichloromethane/methanol mixture without addition of base led to the formation of $[Cu(CH_3OH)_2Cl_2(HL^1)_2]$ (**1**) as green crystals. The crystals must be removed from the mother liquor within 2 days, otherwise colorless crystals of HL^1 will intergrow with the green crystals of **1** rendering the isolation of pure samples impossible. **1** is obtained either when HCl is added to the reaction mixture or from neutral solutions. On the other hand, when NEt_3 is added as a supporting base $[Cu(L^1)_2]$ (**2**) precipitates immediately from the reaction mixture. Compound **2** can also be obtained using copper sources with intrinsically more basic counter anions such as $Cu(Ac)_2\bullet H_2O$ instead of $CuCl_2\bullet2H_2O$, thus avoiding the use of toxic NEt_3. Compound $[Cu(L^2)_2]$ (**3**) was obtained by the reaction of the copper(II) salt with HL^2 in basic condition and using methanol as solvent. Notably, using a dichloromethane/methanol mixture as the solvent prevents the formation of compound **3**. Scheme 1 summarizes the synthetic procedures.

Upon storage at room temperature, complex **1** undergoes a color change from green to brownish-yellow. The color change suggests the methanol loss and subsequent formation of unsolvated complex $[CuCl_2(HL^1)_2]$, as supported by the FT-IR spectrum. The absence of the ν(O-H) stretching band at 3342 cm^{-1} confirms the release of coordinated methanol molecules. Besides, the ν(C=O) vibration, which is at 1670 cm^{-1} in **1**, is split into two bands: 1689 and 1665 cm^{-1}. In addition, the experimental PXRD diffractogram of the resulting solid (Fig. S39) shows the presence of peaks of compound **1** (Fig. S38) and free HL (e.g. peak at 6.61°). Finally, this behavior presumes the decomposition of complex **1** over time.

Instead, compound **2** was isolated. In the FT-IR spectrum of compound **2**, the band at 1456 cm^{-1} corresponds to the ν(C-O) vibration due to deprotonation of HL^1. The ν(C=N) vibration band is seen at 1495 cm^{-1}. In the FT-IR spectrum of compound **3**, the ν(C-O) and ν(C=N) vibration bands are observed at 1447, and 1521 cm^{-1}.

A mixture of crystals of compound **1** and HL^1 was obtained by recrystallizing compound **2** from a methanol/dichloromethane solution and addition of concentrated HCl. Conversely, compound **2** can be regenerated by adding NEt_3 to compound **1** in methanol or in a methanol/dichloromethane mixture.

Compound **1** is centrosymmetric with the metal ion located on an inversion center in a distorted octahedral environment (Fig. 5). Two symmetry related HL^1 ligands coordinate as neutral donors to the Cu^{II} ion through one of the nitrogen atoms of the 1,3,4-thiadiazole ring with Cu1-N2 bond length of 2.0227(14) Å. The charge compensation of the compound is given by the coordination of two chloride ligands (Cu1-Cl1 bond length of 2.2642(5) Å). The methanol molecules are coordinating in the axial positions. The Cu1-O2 distance of 2.6512(15) Å (Table 1) indicate weak bonds of the methanol molecules to the Cu^{II} due to Jahn-Teller effect. In other Cu^{II} complexes containing chloride, methanol and neutral *N*-donor ligands, the Cu-$O_{(MeOH)}$ bond lengths are 2.483(2) [16] and 2.450(2) Å [17], being the metal center Jahn-Teller distorted octahedral. In the Cu^{II} compound obtained by Turner and co-authors, two molecules of methanol are weakly coordinated in the axial positions of the copper and hydrogen bond to the urea oxygen atoms from the neutral ligands [16]. In the complex prepared by Huang and co-authors, the two methanol molecules are weakly coordinated to Cu^{II} center in the axial positions do not engage in hydrogen bonds [17]. Contrastingly, there are N-H•••O and O-H•••N intramolecular hydrogen bonds in compound **1** (Fig. 5, Table S3). Therefore, the elongation in the present case is likely due to accomplish the formation of intramolecular H-bonds. The amide O1-C3 and N3-C3 bond lengths in **1** [1.215(2) and 1.375(2) Å, respectively, Table S4], which are similar to those in free HL^1, confirm the non-involvement of O1 or N3 in the coordination to Cu^{II}.

Compounds **2** and **3** are mononuclear centrosymmetric with the metal ion in a square planar environment (Fig. 6 and Fig. S9). To the best of our knowledge the *N,O*-chelate coordination of ligands having alkyl or aryl groups attached to the carbonyl carbon atom toward Cu^{II} has not been described widely. A somewhat similar example has been reported by *in situ* formation of the ligand through reaction with the released acetate from the metal precursor with 2-amino-1,3,4-thiadiazole [6]. Compound **3** exists as two polymorphs, which are labelled as **3** and **3B**. They crystallized simultaneously from the mother solution as light-green rectangular blocks (**3**) and green blocks (**3B**). In the crystal structure of **2** and **3/3B**, two six membered chelate rings define the geometry of the planar complexes *trans*-$[Cu(L)_2]$. The coordination of anionic $[L^1]^-$ (in **2**) and $[L^2]^-$ (in **3/3B**) through the amidate oxygen atom is confirmed by the elongation of the O1-C3 bond (from ca. 1.22 Å in HL^1 and HL^2) to

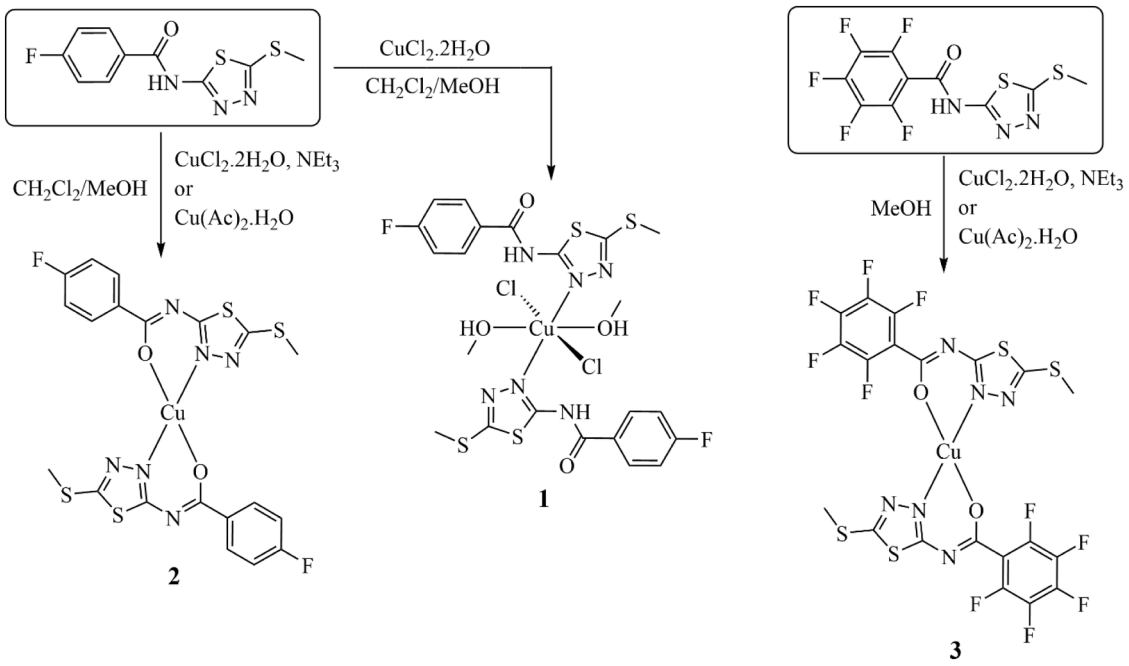

Scheme 1. Preparation procedure of copper(II) complexes **1**−**3**. Reaction condition: r.t., 1 h.

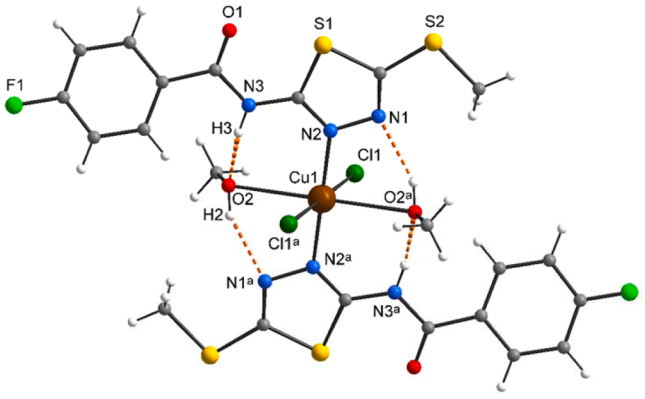

Fig. 5. Molecular structure of compound **1**. Symmetry operator: [a] −*x*, −*y*+1, −*z*+1. Hydrogen bonds are shown in orange dashed lines.

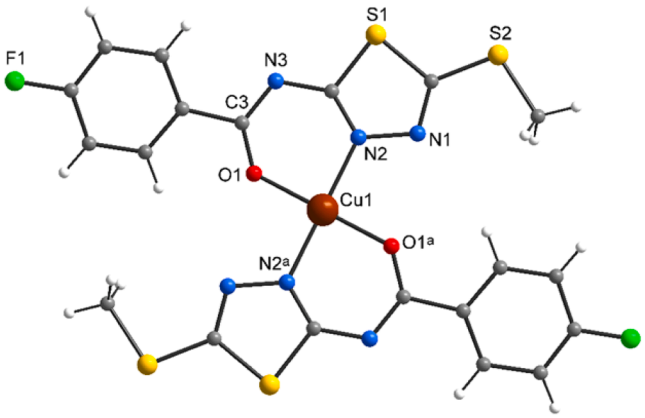

Fig. 6. Molecular structure of compound **2**. Symmetry operator: [a] −*x*+1, −*y*+1, −*z*+1.

Table 1
Selected bond lengths (Å) in compounds **1**−**3**.

	1	2	3/3B
Cu(1)-N(2)	2.0227(14)	1.956(5)	1.9553(17)/1.9655(10)
Cu(1)-O(1)	–	1.898(5)	1.9209(16)/1.9234(9)
Cu(1)-Cl(1)	2.2642(5)	–	–
Cu(1)-O(2)	2.6512(15)	–	–

1.261(8) and 1.272(2)/1.2699(14) Å, and shortening of the N3-C3 bond length (from ca. 1.37 Å in HL[1] and HL[2]) to 1.301(10) and 1.316 (3)/1.3180(15) Å in the complexes (Table S4). Within the deprotonation, the C-O and C-N bonds change it double and simple bond character, as has been illustrated in Scheme 1.

The Cu•••N(thiadiazole) distances between neighboring molecules (3.4210(8) Å in **2**, and 3.5411(12) Å in **3**) are within the sum of the van der Waals radii of the corresponding atoms (3.6 Å [10]), indicating weak interactions (Table 2). Instead of Cu•••N interactions as found in **3**, compound **3B** shows Cu•••S interactions (distance of 3.1133(4) Å). In compounds **2** and **3** (and **3B** polymorph), C-H•••F hydrogen bonds (Table S3) lead to three-dimensional supramolecular networks. Additionally, in compound **2** the packing of the complexes in the solid state structure suggests intermolecular S•••S interactions (distances of 3.4895(8) Å).

As a proof of crystal homogeneity, crystals of compound **1** were ground into a fine powder and the powder X-ray diffractogram was collected. The experimental pattern fits well with the diffractogram generated from the single-crystal X-ray diffraction data (Fig. S38).

Compound **2** precipitated as a microcrystalline solid from the reaction mixture and is barely soluble in polar solvents as DCM and DMSO. Single crystals of **2** were grown by heating a suspension of the obtained powder in DMSO and filtration while hot followed by slow cooling. Although most of the compound precipitated as finely divided deposits, a few larger single crystals were obtained. The simulated powder diffractogram, generated from the single crystal X-ray structure data, differs from the experimental diffractogram obtained from the original microcrystalline precipitate (Fig. S40). Since spectroscopic, spectrometric, and elemental analyses all confirm the same chemical composition, this discrepancy is attributed to the formation of a different polymorph during the slow crystallization process from hot DMSO.

Table 2
Cu•••N, Cu•••S and S•••S interactions in compounds **2** and **3**.

Compound	Interaction(s)	Distance (Å)	Perpendicular view to the chelating donor atoms plane
2	Cu•••N S•••S (see Fig. S8)	3.4210(8) 3.4895(8)	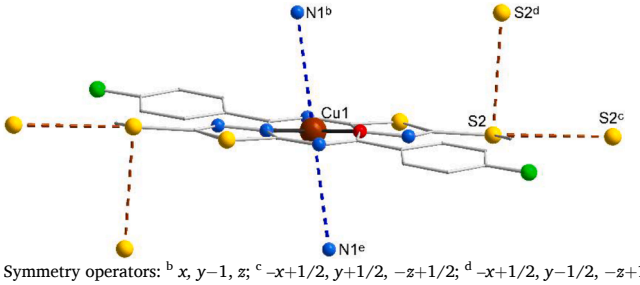 Symmetry operators: [b] *x*, *y*−1, *z*; [c] −*x*+1/2, *y*+1/2, −*z*+1/2; [d] −*x*+1/2, *y*−1/2, −*z*+1/2; [e] −*x*+1, −*y*+2, −*z*+1.
3	Cu•••N (see Fig. S10)	3.5411(12)	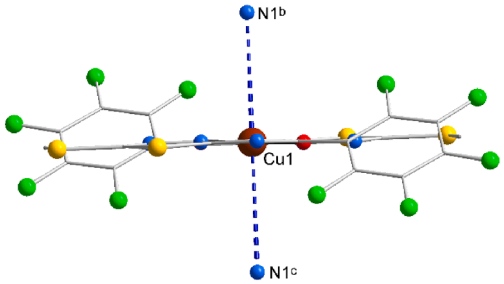 Symmetry operators: [b] *x*+1, *y*, *z*; [c] −*x*, −*y*, −*z*+1.
3B	Cu•••S (see Fig. S11)	3.1133(4)	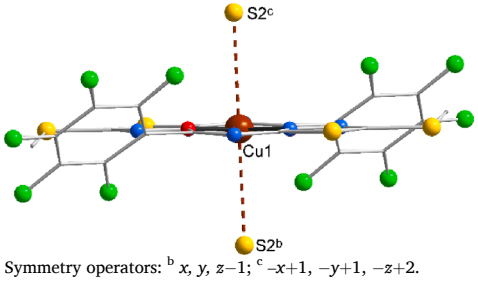 Symmetry operators: [b] *x*, *y*, *z*−1; [c] −*x*+1, −*y*+1, −*z*+2.

The insolubility of compound **2** at room temperature prohibited the recording of UV-Vis spectra of sufficient quality in solution. Therefore, UV-Vis absorption analysis was performed in the solid-state using diffuse reflectance spectroscopy for all the copper(II) compounds. Absorption spectra were obtained from reflectance values using the Kubelka-Munk function, $F(R) = (1\text{-}R)^2/2R$, where R is the reflectance [18]. Fig. S35 shows the corresponding absorption spectra. The n−π* ILCT band is observed centered at 275 (for compound **1**) and 290 nm (for **2** and **3**). The band associated to Cu^{2+} *d-d* transition was observed centered at ca. 730 nm for **1**. For compounds **2** and **3**, the *d-d* transition band was observed at around 630 nm with very low intensity.

Upon dissolution of compound **1** in DMSO (a strongly coordinating solvent), the HL^1 ligand is released and replaced by solvent molecules, as evidenced by UV-Vis and ^{1}H NMR spectra. The UV-Vis and ^{1}H NMR spectra of **1** in DMSO (or DMSO-d_6), recorded several hours after dissolution of a pure solid aliquote of compound **1**, clearly display signals corresponding to free HL^1 (see Fig. S34). Additionally, the ^{1}H NMR spectrum reveals resonances for free methanol at 4.08 and 3.16 ppm (Fig. S23). Line broadening is observed in the spectra due to the paramagnetic nature of Cu(II) ions present in the solution.

The square planar compounds **2** and **3** have their paramagnetic properties confirmed by measurement of solid samples on a magnetic susceptibility balance. The determined effective magnetic moment was 1.65 and 1.73 B.M. for **2** and **3**, respectively, which confirms the spin only (S=½) behavior of 1.73 B.M. for the d^9 configuration. Details about the measurement and calculation of the effective magnetic moments are contained in the *Supplementary Material*.

2.3. A theoretical investigation of close intramolecular S···O contacts

Aroyl thiadiazoles generally show a *cis*-orientation of the sulfur and oxygen atoms featuring somewhat short S•••O contacts that are often attributed to chalcogen bonding. A series of DFT calculations on the B3LYP/def2tzvp were performed with the initial motivation to understand and explain the observed geometries of the aroyl thiadiazole molecules in terms of the resultant topological properties of the electron density in such compounds and investigate the underlying phenomena. For example such interactions would be described by the respective (+3,-1) critical point that is commonly observed between the uncoordinated S and O moieties. Indeed, we located the corresponding critical point, however, a reduced density gradient (RDG) plot for the identification of weak interactions as well as the properties of the electron density at the critical point (for criteria see experimental) suggested this to rather be a weak van der Waals contact instead of the expected chalcogen bond (Figs. S48 and S49).

Intrigued by this observation, we calculated and analyzed a series of hypothetical analogs with sulfur substituted by O, Se, Te, NH, PH, AsH, SbH, BiH, CH_2, SiH_2, GeH_2, SnH_2 and PbH_2 (Fig. S41). The resulting structures show analogous O···E contacts also give rise to corresponding (+3,-1) critical points with similar critical point properties for O, Se, Te, PH, AsH, SbH, BiH, CH_2, SnH_2 and PbH_2 (Table S6, Figs. S42-S47). Thus, such critical points might not actually indicate a relevant favorable bonding interaction but may be the result of a close contact imposed by other geometric or electronic constraints in such systems. This would also be consistent with the low respective NBO orbital contributions to such potential interactions, which are probably best described as weak van der Waals interactions in contrast to the commonly attributed

chalcogen bond. It is noteworthy that corresponding critical points were not located for the SiH_2 and GeH_2 analogs and that the N-H compound gave rise to a hydrogen bond with the neighboring O instead of an O···N contact.

This finding implied the question of the underlying stabilizing effect for the observed *cis*-orientation of S and O in arylamido thiadiazoles if they cannot be explained in terms of an intramolecular O···S chalcogen bond consistently. One possible explanation that was suggested in a related study is the improved π-delocalization of the amido groups electrons into the thiadiazole ring in the *cis*-geometry compared to the *trans*-geometry [9]. This would be enabled by improved angular overlap of the involved orbital lobes of the thiadiazole ring with those of the aroylamide unit and such effects were calculated to be even bigger for deprotonated systems [9].

To further investigate these effects and provide more understanding, we first evaluated the potential tautomers and isomers of the thiadiazole structure (*i.e.* one with an OH instead of NH, one with a 180° flipped thiadiazole ring and one with both changes) (Scheme S1). Surprisingly, while the OH tautomer and the thiadiazole-flipped OH tautomer are stable, only the thiadiazole-flipped isomer is not stable and refines back to the original thiadiazole with *cis*-O,S configuration. All isomers but the *cis*-O,S configured amide structure were energetically less favorable (Table S7). With the original idea of potentially improved delocalization in mind, we determined the isotropic chemical shielding surfaces ($ICSS_{zz}$) for the systems at hand to visualize these differences. A more homogeneous or aromatic distribution of shared electrons will give more or less connected $ICSS_{zz}$ plots, while dearomatization or a heterogeneous distribution of shared electrons will result in a more fragmented $ICSS_{zz}$ (Figs. S50-S55). These plots emphasizes that the delocalized character was maximized in the *cis*-O,S configured amide structure over the alternative isomers. Scans of the $ICSS_{zz}$ for geometry restricted isomers with torsion angles of 60°, 120° and the potentially thiadiazole-inverted 180° rotated structures all showed decreased delocalization between the amide group and the thiadiazole moiety. The effect of adjusting the electron density at the amide moiety – in this case through hydrogen bonding with a second analogously oriented, identical molecule – was considered next. The weakening of the N-H bond clearly increased the electron density at O (Figs. S56 and S57), increasing its interaction with S according to an RDG analysis (Fig. S58, Table S8). A side-by-side graphical comparison of the properties in the RDG of the monomeric and hydrogen-bonded, dimeric structures of HL^1 are shown in Fig. 7.

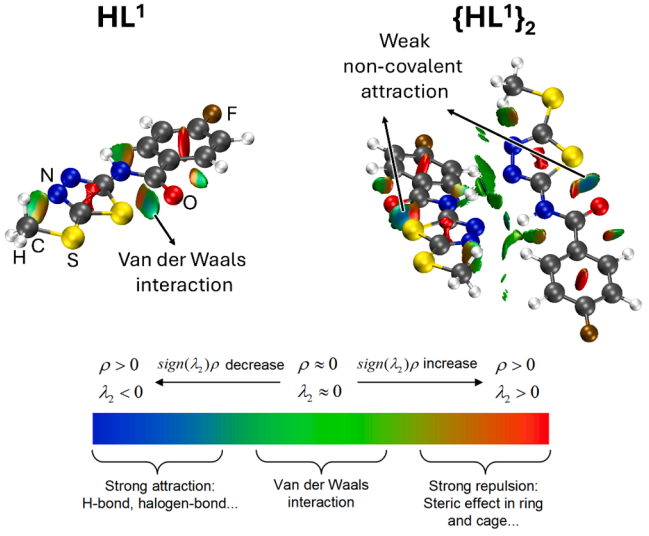

Fig. 7. Reduced density gradient (RDG) of monomeric (left) and hydrogen-bonded, dimeric (right) HL^1. Red color corresponds to repulsive interactions (e.g. in the center of a delocalized aromatic ring system), blue represents constructive non-covalent interaction (e.g. hydrogen bonding) and green is indicative of van der Waals contacts.

While the energetic preference for a *cis* orientation of the carboxamide oxygen atom and the thiadiazole rings sulfur atom is clearly enhanced by intramolecular hydrogen bonding, an additional stabilization by crystal packing requirements cannot be excluded. Therefore, it can be assumed that improved delocalization might be a much better suited, underlying explanation for the *cis*-orientation in uncoordinated amidothiadiazoles compared to the previously assumed intramolecular chalcogen-bonding in some cases. However, the situation is complex and a dedicated, more thorough theoretical study would be required to shed further light on this issue in a generalizable way.

2.4. Assessment of cell viability and cytotoxicity

Cytotoxicity assays are crucial for the preliminary biological evaluation of novel compounds. Accordingly, the cytotoxic effects of ligands HL^1, HL^2 as well as their corresponding copper complexes **1** and **3** were investigated. Table 3 summarizes the cytotoxic concentration at 50% (CC_{50}) against MCF-7 cell line (human breast cancer epithelial ER+/PR+) and HaCaT cell lines (immortalized human epidermal keratinocyte) after 48 h of treatment. The assay was performed using a serial dilution starting from 25 μM of HL^1, HL^2 and complexes **1** and **3**. The corresponding dose-response curves from replicate experiments are shown in Fig. S59. Complex **2** exhibited low/poor solubility, which prevented its *in vitro* evaluation under the same experimental conditions. The cell viability percentage was measured by standard MTT [3-(4,5-dimethylthiazol-2-yl)-2,5-diphenyltetrazolium bromide] evaluation.

Ligands HL^1 and HL^2 were non cytotoxic at tested concentrations range in either cell lines, while complexes **1** and **3** presented cytotoxicity in low micromolar range. The selectivity indices (SI ≈ 2) for both complexes indicate low selectivity, and their CC_{50} values were statistically indistinguishable.

As previously discussed, complex **1** undergoes ligand exchange in DMSO solution, as evidenced by UV-Vis spectroscopy. To investigate how this property influences the biological outcome, a simple mixture of HL^1 and $CuCl_2{\bullet}2H_2O$ in 2:1 molar ratio was tested under the same conditions. As observed on Table 3, this mixture is less toxic than complex **1**, suggesting that the metal coordination is essential to the biological outcome. Despite the ligand exchange, complex **1** is significantly more cytotoxic than a simple mixture of Cu(II) and HL^1.

Using the same experimental methodology, cisplatin exhibited CC_{50} values of 13.9 ± 2.0 μM after 48 h of incubation and 4.8 ± 0.8 μM after 72 h in MCF-7 cells. Under comparable conditions, compounds **1** and **3** demonstrated significantly higher cytotoxicity than cisplatin [19–21].

Copper(II) complexes bearing structurally related ligands, such as 1,3,4-thiadiazoles, have also been evaluated against the MCF-7 cell line. For example, a Cu(II)–1,3,4-thiadiazole complex showed a CC_{50} value of 9.71 ± 1.18 μM, compared with 2.37 ± 0.05 μM for the corresponding free ligand [22]. In contrast, several 1,3,4-thiazole derivatives displayed CC_{50} values around 50 μM, corroborating the generally low cytotoxicity associated with this class of ligands [23]. Additionally, the Cu(II) complex of saccharinate-2,6-bis(2-benzimidazolyl) exhibited a CC_{50} value of

Table 3
In vitro cytotoxic concentration at 50% (CC_{50}) against MCF-7 and HaCaT cells after 48 h treatment with HL^1, HL^2, **1** and **3**. SI: CC_{50} (HaCaT)/ IC_{50} (MCF-7). SD calculates from three independent experiments.

Compound	MCF-7 CC_{50} (μM)	HaCaT CC_{50} (μM)
HL^1	>25	>25
HL^2	>25	>25
1	5.02 ± 1.97	9.10 ± 0.58
3	3.00 ± 1.78	7.88 ± 2.16
$CuCl_2{\bullet}2H_2O$ + $2HL^1$	23.20	>25

2.96 ± 0.06 μM in MCF-7 cells under similar experimental conditions [21]. Likewise, Cu(II)–fluorobenzyloxychalcone complexes showed enhanced cytotoxicity, with CC_{50} values of approximately 1.0 μM, compared with 10 μM for the corresponding free ligands [24].

Overall, the CC_{50} values obtained in this study are in good agreement with those reported in the literature for Cu(II) complexes evaluated under comparable conditions in MCF-7 cells, supporting the relevance and consistency of the present findings.

3. Experimental

3.1. Materials and apparatus

Fourier transform infrared (FT-IR) spectra were measured on a Bruker VERTEX 70 spectrometer between 200 and 4000 cm^{-1} (resolution of 4 cm^{-1}) in the ATR mode. Elemental analysis of carbon, hydrogen, nitrogen and sulfur were determined using a Heraeus vario EL, or PerkinElmer 2400 series II elemental analyzer. Electrospray ionization (ESI) high-resolution mass spectrometry (HRMS) was used for acquisition of mass spectra on an Agilent 6210 ESI-TOF or a Schimadzu Q-TOF LCMS-9050 spectrometer (positive mode). All MS results are given in the form *m/z* assignment. ^{1}H, ^{13}C and ^{19}F NMR spectra for HL^1 and HL^2 were taken with a Bruker 600.13 MHz (for ^{1}H nuclei) BioSpin GmbH spectrometer. ^{1}H and ^{19}F NMR spectra for **1** were taken with a JEOL ECA 400.53 MHz (for ^{1}H nuclei) spectrometer. DMSO-d_6 was used as solvent. Chemical shifts were referenced to the resonance of the residual solvent protons. Fluorescence measurements of HL^1 and HL^2 were performed using a Horiba FluoroMax Plus spectrofluorometer with excitation and emission slits of 2.0 or 5.0 nm for the collection of the excitation and emission spectra. The UV-Vis spectra of HL^1, HL^2 and compound **1** were collected on a Shimadzu UV-2600 spectrophotometer using DMSO as solvent. The diffuse reflectance (DR) spectra of compounds **1**−**3** were recorded in a Shimadzu UV-2600 spectrophotometer equipped with a diffuse reflectance accessory (integrating sphere ISR 2600 Plus). Barium sulphate was used as white reference material. The DRS-UV-Vis spectra were calculated using the Kubelka-Munk treatment of the DR data [18]. Magnetic susceptibility measurements were performed on a Johnson Matthey Magnetic Susceptibility Balance Mark 1 (S/N: 19670) for compounds **2** and **3** in the solid-state. The balance was recalibrated with solid $Hg[Co(SNC)_4]$. Diamagnetic correction was calculated using the Pascal constants from Bain & Berry [25].

Single-crystal diffraction data collection for HL^1 was obtained using a STOE IPDS 2T instrument with Mo-Kα radiation (λ = 0.71073 Å). The diffraction data collection for compounds **1** and **2** were obtained using a Bruker D8 QUEST ECO diffractometer with graphite monochromated Mo-Kα radiation (λ = 0.71073 Å) and a Photon II detector. The diffraction data collection for HL^2 and compound **3** were obtained using a Bruker D8 VENTURE diffractometer with graphite monochromated Mo-Kα radiation (λ = 0.71073 Å) and a Photon 100 detector. The structures were solved using dual space method using Bruker XT and refined with Bruker XL on F^2 using anisotropic thermal parameters for all non-hydrogen atoms. The hydrogen atom positions were calculated starting from the geometric idealized positions. Data collection and structure refinement parameters, and the crystallographic data are given in Tables S1-S2. The anisotropic thermal ellipsoid plots of the compounds are in Figs. S1–S6. Additional information on the structure determination has been deposited with the Cambridge Crystallographic Data Centre (CCDC 2496200 - 2496205). These data can be obtained free of charge via www.ccdc.cam.ac.uk/structures.

The 2-amino-5-(methylthio)-1,3,4-thiadiazole was prepared from 5-amino-1,3,4-thiadiazole-2-thiol, according to the literature [26].

3.2. Computational details

DFT calculations were performed on the high-performance computing systems of the Freie Universität Berlin ZEDAT (Curta) [27] using the program package GAUSSIAN 16 [28]. The gas phase geometry optimization was performed using coordinates derived from the X-ray crystal structures using GAUSSVIEW and Avogadro [29,30]. The calculations were performed with the hybrid density functional B3LYP [31–33]. The triple-ζ (pseudo)potential basis set def2-TZVP was used for all atoms [34–36]. The basis sets as well as the ECPs were obtained from the basis set exchange database [37]. Further analyses were performed with the free multifunctional wavefunction analyzer *Multiwfn* [38]. Details about the applied criteria for the classification of weak interactions based on topological descriptors are given in [39–42].

3.3. Cell viability tests protocol

Cell viability was evaluated by means of the MTT assay, according to a previously described protocol with adaptations [43,44]. The MCF 7 (human breast cancer ER+/PR+) and HaCaT non-tumor cell lines (immortalized human keratinocytes) were used. The cells were seeded in 96 well plates at a density of 5.10^4 cells/well, in 100 μL of suitable culture medium (DMEM/F-12 high glucose, supplemented with 10% FBS and 1% antibiotic). After 24 h of incubation at 37 °C with 5% CO_2 for cell adhesion, the compounds were added in different concentrations (0.39 to 25 μM), diluted in culture medium with a maximum of 0.25% DMSO (v/v). After 48 h of treatment, 23 μL of MTT solution (5 mg/mL in PBS) was added to each well and the cells were incubated for another 4 h. Next, the medium was carefully removed, and the formazan crystals were solubilized with 100 μL of DMSO. Absorbance was measured at 570 nm using a microplate reader (Varioskan multimode plate reader Thermo Fisher Scientific). The data were expressed as a percentage of cell viability in relation to the negative control (cells treated only with DMSO) and plotted versus the compound concentration. All experiments were carried out in biological and experimental triplicate.

3.4. Syntheses

Preparation of 4-fluoro-*N*-(5-(methylthio)-1,3,4-thiadiazol-2-yl) benzamide (HL^1)

In a 100 mL two-necked flask, under inert atmosphere, 4-fluorobenzoyl chloride (1.58 g [1.18 mL], 10.0 mmol), 2-amino-5-(methylthio)-1,3,4-thiadiazole (1.47 g, 10 mmol) and 20 mL of dry THF were added. NEt_3 (2.09 mL, 15.0 mmol) was poured into an addition funnel, dissolved in 10 mL of dry THF, and added dropwise to the mixture in the flask. After the complete addition of NEt_3, the reaction mixture was stirred at 40 °C during 4 h. The precipitate was filtered off, washed with 100 mL of distilled water (removal of $[Et_3NH]Cl$) and 15 mL of cold ethanol, and air-dried. The crude product was recrystallized in a CH_2Cl_2/MeOH mixture (1:1 *v/v*) yielding a white microcrystalline solid, which was filtered off and dried. Yield: 90% based on 2-amino-5-(methylthio)-1,3,4-thiadiazole. ESI(+)-MS (in MeOH, *m/z*): $[HL^1 + Na]^+$ 291.9992 (calc.: 291.9985). ^{1}H NMR (600.13 MHz, DMSO-d_6): δ 13.13 (s, 1H, >NH), 8.21-8.15 (m, 2H, >CH), 7.39 (t, J = 8.8 Hz, 2H, >CH), 2.74 (s, 3H, -CH_3). ^{13}C NMR (150.90 MHz, DMSO-d_6): δ 164.9 (d, $^{1}J_{C\text{-}F}$ = 251.4 Hz, CF), 164.2 (C=O), 160.7 (C=N), 159.3 (C=N), 131.4 (d, $^{3}J_{C\text{-}F}$ = 9.4 Hz, CH), 128.0 (C=C), 115.8 (d, $^{2}J_{C\text{-}F}$ = 22.1 Hz, CH), 15.9 (CH_3). ^{19}F NMR (564.63 MHz, DMSO-d_6): δ –106.3. UV-Vis (DMSO): λ 299 nm (ε 12006 L mol^{-1} cm^{-1}). FT-IR (ATR, ν_{max} in cm^{-1}): 3147 [ν(NH)], 1661 [ν(C=O)], 1593 [ν(C=C)], 1528 [ν(C=N)], 1505 [δ(CNH)], 1432 [ν(CS)].

Preparation of 2,3,4,5,6-pentafluoro-*N*-(5-(methylthio)-1,3,4-thiadiazol-2-yl)benzamide (HL^2)

The preparation procedure was the same used for HL^1 by using 2,3,4,5,6-pentafluorobenzoyl chloride as reactant instead of 4-fluorobenzoyl chloride. Yield: 71% based on 2-amino-5-(methylthio)-1,3,4-thiadiazole. ESI(+) MS (in CH_3CN/DMSO, *m/z*): $[HL^2 + H]^+$ 341.9806 (calc.: 341.9789), $[HL^2 + Na]^+$ 363.9628 (calc.: 363.9608). ^{1}H NMR (600.13 MHz, DMSO-d_6): δ 13.84 (s, 1H, >NH), 2.75 (s, 3H, -CH_3). ^{13}C NMR (150.90 MHz, DMSO-d_6): δ 162.0 (C=N), 157.9 (C=O), 156.3

(C=N), 143.7 (d, $^{1}J_{C\text{-}F}$ = 251.0 Hz, CF), 142.4 (d, $^{1}J_{C\text{-}F}$ = 255.1 Hz, CF), 137.2 (d, $^{1}J_{C\text{-}F}$ = 251.3 Hz, CF), 109.8 (C=C), 16.0 (CH_3). ^{19}F NMR (564.63 MHz, DMSO-d_6): δ –140.3, –149.7, –160.7. UV-Vis (DMSO): λ 299 nm (ε 11509 L mol^{-1} cm^{-1}). FT-IR (ATR, ν_{max} in cm^{-1}): 3188 [ν(NH)], 1695 [ν(C=O)], 1653 [ν(C=C)], 1575 [ν(C=N)], 1496 [δ(CNH)], 1421 [ν(CS)].

Synthesis of $[Cu(CH_3OH)_2Cl_2(HL^1)_2]$ (1)

In a 50 mL flask, HL^1 (108 mg, 0.40 mmol) was dissolved in 20 mL of a CH_2Cl_2/MeOH mixture (1:1 *v/v*). One drop of concentrated HCl was added, producing a white suspension of $[H_2L^1]Cl$. Solid $CuCl_2\bullet 2H_2O$ (75 mg, 0.44 mmol) was added. After 1 h, the mixture was filtered through Celite® for the removal of remaining particles, and the lime green solution was stored at 15 °C. Within one or two days, the green crystals (rectangular blocks) of **1** were isolated and air-dried. Yield: 49% based on HL^1. Elemental Analysis: calc. for $C_{22}H_{24}Cl_2CuF_2N_6O_4S_4$: C, 35.85; H, 3.28; N, 11.40; found: C, 35.88; H, 2.90; N, 10.83. ESI(+) MS (in CH_2Cl_2, *m/z*): $[Cu(HL^1)(L^1)]^+$ 599.9397 (calc. 599.9403), $[Cu(HL^1)_2(L^1)]^+$ 868.9459 (calc. 868.9496), $[Cu_2(L^1)_3]^+$ 931.8600 (calc. 931.8618). ^{1}H NMR (400.53 MHz, DMSO-d_6): δ 8.17 (s, 4H, >CH), 7.38 (s, 4H, >CH), 4.08 (s, 2H, -OH), 3.16 (s, 6H, -CH_3), 2.73 (s, 6H, -CH_3). ^{19}F NMR (376.84 MHz, DMSO-d_6): δ –106.1. FT-IR (ATR, ν_{max} in cm^{-1}): 3342 [ν(OH)], 1670 [ν(C=O)], 1602 [ν(C=C)], 1551 [ν(C=N)], 1512 [δ(CNH)].

Synthesis of $[Cu(L^1)_2]$ (2)

In a 50 mL flask, HL^1 (108 mg, 0.40 mmol) was dissolved in 20 mL of a CH_2Cl_2/MeOH mixture (1:1 *v/v*). Solid $CuCl_2\bullet 2H_2O$ (75 mg, 0.44 mmol) was added. Then, three drops of NEt_3 were added. The mixture was stirred at room temperature for 1 h. The brownish green solid was filtered off, washed with hot methanol and air-dried. Yield: 97% based on HL^1. Elemental Analysis: calc. for $C_{20}H_{14}CuF_2N_6O_2S_4$: C, 40.03; H, 2.35; N, 14.00; found: C, 39.76; H, 2.19; N, 13.62. ESI(+) MS (in CH_2Cl_2, *m/z*): $[Cu(L^1)_2 + H]^+$ 599.9420 (calc. 599.9403), $[Cu(L^1)_3 + H]$ 868.9488 (calc. 868.9496), $[Cu_2(L^1)_3]^+$ 931.8614 (calc. 931.8618), $[Cu_2(L^1)_4 + H]^+$ 1200.8706 (calc. 1200.8707). FT-IR (ATR, ν_{max} in cm^{-1}): 1601 [ν(C=C)], 1495 [ν(C=N)], 1456 [ν(C−O)].

Single-crystals were obtained within recrystallization in hot dimethyl sulfoxide.

Synthesis of $[Cu(L^2)_2]$ (3)

In a 50 mL flask, HL^2 (136 mg, 0.40 mmol) and $CuCl_2\bullet 2H_2O$ (38 mg, 0.22 mmol) were suspended in 5 mL of MeOH. Three drops of NEt_3 were added, producing a clear green solution. Within 1-2 min precipitate was observed. The mixture was stirred at room temperature for 1 h. The light green solid was filtered off, washed with methanol and air-dried. Yield: 94% based on HL^2. Elemental Analysis: calc. for $C_{20}H_6CuF_{10}N_6O_2S_4$: C, 32.28; H, 0.81; N, 11.29; found: C, 32.71; H, 0.82; N, 11.28. ESI(+) MS (in MeOH/$CHCl_3$, *m/z*): $[Cu(L^2)_2 + H]^+$ 743.8679 (calc. 743.8644), $[Cu(L^2)_2 + Na]^+$ 765.8502 (calc. 765.8464). FT-IR (ATR, ν_{max} in cm^{-1}): 1649 [ν(C=C)], 1521 [ν(C=N)], 1447 [ν(C−O)].

Single-crystals of two polymorphs (**3** and **3B**) were obtained from the mother solution.

4. Conclusion

4-fluoro-*N*-(5-(methylthio)-1,3,4-thiadiazol-2-yl)benzamide (HL^1) and 2,3,4,5,6-pentafluoro-*N*-(5-(methylthio)-1,3,4-thiadiazol-2-yl)benzamide (HL^2) have planar *O,S cis*-orientation. This configuration was also observed in the coordinated molecule to Cu^{II} ion in $[Cu(CH_3OH)_2Cl_2(HL^1)_2]$ (**1**) through one nitrogen atom from the thiadiazole ring. Deprotonation of HL^1 or HL^2 led to the formation of $[Cu(L^1)_2]$ (**2**) and $[Cu(L^2)_2]$ (**3**), and *N,O*-chelates were observed, thus losing the *O, S cis* orientation. Compound **1** decomposes slowly in the solid-state and loses its identity by dissolution in DMSO. Compound **2** is hardly soluble even in hot DMSO while compound **3** is well soluble in several solvents such as DCM, ACN, DMF and DMSO. Complexes **1** and **3** are cytotoxic against carcinogenic MCF-7 cells while the free HL^1 and HL^2 ligands were non-cytotoxic under the same conditions. The complex **1** has a distinct biological outcome than the simple mixture of Cu(II) salt and HL^1, suggesting that the coordination complex itself is responsible for the cytotoxic effect rather than the release of Cu(II) ions from the complex in solution. Although both complexes present antitumor effects against MCF-7, they present low selectivity indices when compared to their effects on the non-tumorigenic HaCaT cell line.

CRediT authorship contribution statement

Ana Júlia Zimmermann Londero: Methodology, Investigation, Formal analysis, Data curation. **Ulrich Abram:** Funding acquisition, Formal analysis. **Maximilian Roca Jungfer:** Investigation, Data curation. **Gabriela Nanci Ledesma:** Formal analysis, Data curation. **Jennyfer Castro:** Investigation, Formal analysis. **Camilla Abbehausen:** Resources, Investigation, Formal analysis. **Vânia Denise Schwade:** Writing – review & editing, Writing – original draft, Supervision, Conceptualization.

Declaration of competing interest

The authors declare that they have no known competing financial interests or personal relationships that could have appeared to influence the work reported in this paper.

Acknowledgments

The authors gratefully acknowledge the financial support provided by the Brazilian agencies CAPES (Coordenação de Aperfeiçoamento de Pessoal de Nível Superior – Programa de Demanda Social) – process number 88887.466685/2019-00, and CAPES/PROBRAL Program – process number 88887.665129/2022-00. M. R. J. gratefully acknowledges the financial support from VCI Liebig fellowship of Fonds der Chemischen Industrie. The X-ray diffraction and the spectroscopy facilities were acquired with support from FINEP/CT-Infra. The authors also acknowledge Prof. Dr. Robert Alan Burrow for the magnetic susceptibility measurements and calculation of the effective magnetic moment.

Supplementary materials

Supplementary material associated with this article can be found, in the online version, at doi:10.1016/j.molstruc.2026.145427.

Data availability

Data will be made available on request.

References

[1] K. Sonawane, R. Said, N. Hatvate, Chapter 7: Synthesis, Properties, and Biological Applications of 1,3,4-Thiadiazoles, In: S-Heterocycles: Retrospect, Prospects, and Biological Applications, RSC Books 2024 163–223, doi:10.1039/9781837674015-00163.

[2] Y. Hu, C.-Y. Li, X.-M. Wang, Y.-H. Yang, H.-L. Zhu, 1,3,4-Thiadiazole: synthesis, reactions, and applications in medicinal, agricultural, and materials chemistry, Chem. Rev. 114 (2014) 5572–5610, https://doi.org/10.1021/cr400131u.

[3] A.K. Jain, S. Sharma, A. Vaidya, V. Ravichandran, R.K. Agrawal, 1,3,4-Thiadiazole and its derivatives: a review on recent progress in biological activities, Chem. Biol. Drug Des. 81 (2013) 557–576, https://doi.org/10.1111/cbdd.12125.

[4] S.S. Tandon, L. Chen, L.K. Thompson, J.N. Bridson, Dinuclear copper(II) complexes of the tetradentate thiadiazole ligands BPMTD (2,5-bis((2-pyridylmethyl)thio) thiadiazole) and BPTD (2,5-bis(2-pyridylthio)thiadiazole). X-ray structures of $[Cu_2(BPTD)(\mu_2\text{-}Br)_2Br_2]$ and $[Cu(BPMTD)Cl_2]_n$ and spectroscopic, electrochemical, and magnetic studies, Inorg. Chem. 33 (1994) 490–497, https://doi.org/10.1021/ic00081a016.

[5] J.-L. Song, Z.-C. Dong, H.-Y. Zeng, W.-B. Zhou, T. Naka, Q. Wei, J.-G. Mao, G.-C. Guo, J.-S. Huang, $[Cu(H_4C_3N_2S)Cl_2]_n$, an Unprecedented diazole-bridged one-dimensional copper halide: synthesis, structure, and magnetic properties, Inorg. Chem. 42 (2003) 2136–2140, https://doi.org/10.1021/ic025976m.

[6] R.K. Dani, M.K. Bharty, S.K. Kushawaha, O. Prakash, R.K. Singh, N.K. Singh, Ni(II), Cu(II) and Zn(II) complexes of (Z)-N'(1,3,4-thiadiazol-2-yl)acetimidate: Synthesis,

spectral, solid state electrical conductivity, X-ray diffraction and DFT study, Polyhedron 65 (2013) 31–41, https://doi.org/10.1016/j.poly.2013.08.015.
[7] Kang S.K., Cho N.S., Jeon M.K. N-(5-Eth-oxy-1,3,4-thia-diazol-2-yl)benzamide. Acta Crystallogr. Sect. E Struct. Rep. Online 68(Pt 2) (2012) o544. doi:10.1107/S1600536812002978.
[8] N.S. Cho, H.J. Hwang, J.-G. Kim, I-H. Suh, Regiospecific alkylation of 5-substituted 2-acylamino-1,3,4-thiadiazoles, Heterocycles 55 (2001) 579–587, https://doi.org/10.3987/COM-00-9147.
[9] A.J.Z. Londero, U. Abram, M.R. Jungfer, V.D. Schwade, Cu^{II} and Zn^{II} Complexes with 1,3,4-Thiadiazole-5-Thiomethyl-Based Diamide, Eur. J. Inorg. Chem. 28 (2025) e202400736, https://doi.org/10.1002/ejic.202400736.
[10] S.S. Batsanov, Van der Waals radii of elements, Inorg. Mater. 37 (2001) 871–885, https://doi.org/10.1023/A:1011625728803.
[11] T. Ghosh, P. Maity, B.C. Ranu, Cobalt-catalyzed remote C-4 functionalization of 8-aminoquinoline amides with ethers via C−H activation under visible-light irradiation. Access to α-Heteroarylated ether derivatives, Org. Lett. 20 (2018) 1011–1014, https://doi.org/10.1021/acs.orglett.7b03955.
[12] N. Łukasik, E. Luboch, J. Chojnacki, E. Wagner-Wysiecka, 1,3,4-Thiadiazole-based diamides: synthesis and complexation properties, J. Mol. Struct. 1146 (2017) 713–722, https://doi.org/10.1016/j.molstruc.2017.06.057.
[13] T.T. Toshmurodov, A.A. Ziyaev, B.Z. Elmuradov, D.S. Ismailova, E.R. Kurbanova, Highly selective synthesis and fungicidal activity of the Novel 2-Alkylthio-5-Amino-1,3,4-Thiadiazoles, J. Chem. Chem. Sci. 6 (2016) 199–204.
[14] T.A. Mohamed, U.A. Soliman, I.A. Shaaban, W.M. Zoghaib, L.D. Wilson, Raman, infrared and NMR spectral analysis, normal coordinate analysis and theoretical calculations of 5-(methylthio)-1,3,4-thiadiazole-2(3H)-thione and its thiol tautomer, Spectrochim. Acta A 150 (2015) 339–349, https://doi.org/10.1016/j.saa.2015.05.039.
[15] M.K. Bharty, A. Bharti, R.K. Dani, S.K. Kushawaha, R. Dulare, N.K. Singh, Studies on novel Cu(II) complexes of 5-(4-hydroxy-phenyl)-1,3,4-thiadiazole-2-thiol and 5-thiophen-2-yl-3H-1,3,4-oxadiazole-2-thione: synthesis, spectral and structural characterization, Polyhedron 41 (2012) 52–60, https://doi.org/10.1016/j.poly.2012.04.025.
[16] D.R. Turner, B. Smith, A.E. Goeta, I.R. Evans, D.A. Tocher, J.A.K. Howard, J. W. Steed, The $R_1^2(6)$ hydrogen-bonded synthon in neutral urea and metal-bound halide systems, CrystEngComm (6) (2004) 633–641, https://doi.org/10.1039/B415627G.
[17] X. Huang, Y. Xia, H. Zhang, Z. Yan, Y. Tang, X.-J. Yang, B. Wu, Synthesis, crystal structure, and fluorescence studies of (1-naphthyl)(pyridyl)urea metal complexes, Inorg. Chem. Commun. 11 (2008) 450–453, https://doi.org/10.1016/j.inoche.2008.01.021.
[18] S. Nilavazhagan, D. Anbuselvan, A. Santhanam, N. Chidhambaram, Effect of an alkali hydroxide concentration on the structural, optical, and surface morphological properties of ZnO nanoparticles, Appl. Phys. A 126 (2020) 279, https://doi.org/10.1007/s00339-020-3462-3.
[19] A.M.R. Polez, R.L. Farias, A.A. de Lima, A.B. Lazzarini, T.R. de Moura, J. M. Velasques, J.C. Souza, F.V. Rocha, M.A. Lima, J. Ellena, V.M. Miranda, V. M. Deflon, M.B. Moreira, A.V.G. Netto, Oxime-derived palladacycles bearing 2,6-lutidine: Synthesis, cytotoxicity evaluation and interactions with biomolecules, J. Mol. Struct. 1321 (2025) 140232, https://doi.org/10.1016/j.molstruc.2024.140232.
[20] C. Abbehausen, E.J. Peterson, R.E.F. de Paiva, P.P. Corbi, A.L.B. Formiga, Y. Qu, N. P. Farrell, Gold(I)-Phosphine-N-Heterocycles: biological activity and specific (Ligand) Interactions on the C-Terminal HIVNCp7 Zinc finger, Inorg. Chem. 52 (2013) 11280–11287, https://doi.org/10.1021/ic401535s.
[21] C. Icsel, V.T. Yilmaz, Ş. Aydinlik, M. Aygun, New manganese(II), iron(II), cobalt (II), nickel(II) and copper(II) saccharinate complexes of 2,6-bis(2-benzimidazolyl) pyridine as potential anticancer agents, Eur. J. Inorg. Chem. 202 (2020) 112535, https://doi.org/10.1016/j.ejmech.2020.112535.
[22] B.-L. Fei, S. Tu, Z. Wei, P. Wang, J.-Y. Long, C. Qiao, Z.-F. Chen, Biological evaluation of optically pure chiral binuclear copper(II) complexes based on a rosin derivative as highly potential anticancer agents, Dalton Trans. 48 (2019) 15646–15656, https://doi.org/10.1039/C9DT01942A.
[23] S. Janowska, D. Khylyuk, A. Bielawska, A. Szymanowska, A. Gornowicz, K. Bielawski, J. Noworól, S. Mandziuk, M. Wujec, New 1,3,4-Thiadiazole derivatives with anticancer activity, Molecules 27 (6) (2022) 1814, https://doi.org/10.3390/molecules27061814.
[24] L.S. Oliveira, P.H.S. Guarda, L.B. Rosa, G.C. Rodrigues, D.D. Affonso, J.E. de Carvalho, I.A. Santos, M. Harris, D.H. Nakahata, J.R. Sabino, D.C. Miguel, A.L.T. G. Ruiz, A.C.G. Jardim, C. Abbehausen, Exploring the copper(II) coordination to 2′-hydroxy-4-benzyloxychalcone analogues and their potential pharmacological applications, Inorg. Chim. Acta 560 (2024) 121806, https://doi.org/10.1016/j.ica.2023.121806.
[25] G.A. Bain, J.F. Berry, Diamagnetic Corrections and Pascal's Constants, J. Chem. Ed. 85 (2008) 532–536, https://doi.org/10.1021/ed085p532.
[26] P. Ortega-Luoni, L. Vera, C. Astudillo, M. Guzmán, P. Ortega-López, Synthesis of metallic azoderivatives of 2-amino-5-mercapto-1,3,4-thiadiazole, J. Chil. Chem. Soc. 52 (1) (2007) 1120–1122, https://doi.org/10.4067/S0717-97072007000100015.
[27] High performance computing (HPC) system Curta at Freie Universität Berlin.
[28] Revision B.01, M.J. Frisch, G.W. Trucks, H.B. Schlegel, G.E. Scuseria, M.A. Robb, J. R. Cheeseman, G. Scalmani, V. Barone, G.A. Petersson, H. Nakatsuji, X. Li, M. Caricato, A.V. Marenich, J. Bloino, B.G. Janesko, R. Gomperts, B. Mennucci, H. P. Hratchian, J.V. Ortiz, A.F. Izmaylov, J.L. Sonnenberg, D. Williams-Young, F. Ding, F. Lipparini, F. Egidi, J. Goings, B. Peng, A. Petrone, T. Henderson, D. Ranasinghe, V.G. Zakrzewski, J. Gao, N. Rega, G. Zheng, W. Liang, M. Hada, M. Ehara, K. Toyota, R. Fukuda, J. Hasegawa, M. Ishida, T. Nakajima, Y. Honda, O. Kitao, H. Nakai, T. Vreven, K. Throssell, J.A.Jr. Montgomery, J.E. Peralta, F. Ogliaro, M.J. Bearpark, J.J. Heyd, E.N. Brothers, K.N. Kudin, V.N. Staroverov, T. A. Keith, R. Kobayashi, J. Normand, K. Raghavachari, A.P. Rendell, J.C. Burant, S. S. Iyengar, J. Tomasi, M. Cossi, J.M. Millam, M. Klene, C. Adamo, R. Cammi, J. W. Ochterski, R.L. Martin, K. Morokuma, O. Farkas, J.B. Foresman, D.J. Fox, Gaussian 16, Gaussian, Inc., Wallingford CT, 2016. Revision B.01,.
[29] GaussView, Version 6, R. Dennington; T. A. Keith; and J. M. Millam, Semichem Inc., Shawnee Mission, KS, 2016.
[30] M.D. Hanwell, D.E. Curtis, D.C. Lonie, C. Vandermeersch, E. Zurek, G.R. Hutchison, Avogadro: an advanced semantic chemical editor, visualization, and analysis platform, J. Cheminform. 4 (2012) 17, https://doi.org/10.1186/1758-2946-4-17.
[31] S.H. Vosko, L. Wilk, M. Nusair, Accurate spin-dependent electron liquid correlation energies for local spin density calculations: a critical analysis, Can. J. Phys. 58 (8) (1980) 1200–1211, https://doi.org/10.1139/p80-159.
[32] A.D. Becke, Density-functional thermochemistry. III. The role of exact exchange, J. Chem. Phys. 98 (7) (1993) 5648–5652, https://doi.org/10.1063/1.464913.
[33] C. Lee, W. Yang, R.G. Parr, Development of the Colle-Salvetti correlation-energy formula into a functional of the electron density, Phys. Rev. B 37 (1988) 785–789, https://doi.org/10.1103/PhysRevB.37.785.
[34] F. Weigend, R. Ahlrichs, Balanced basis sets of split valence, triple zeta valence and quadruple zeta valence quality for H to Rn: design and assessment of accuracy, Phys. Chem. Chem. Phys. 7 (2005) 3297–3305, https://doi.org/10.1039/B508541A.
[35] K.A. Peterson, D. Figgen, E. Goll, H. Stoll, M. Dolg, Systematically convergent basis sets with relativistic pseudopotentials. II. Small-core pseudopotentials and correlation consistent basis sets for the post-d group 16–18 elements, J. Chem. Phys. 119 (21) (2003) 11113–11123, https://doi.org/10.1063/1.1622924.
[36] B. Metz, H. Stoll, M. Dolg, Small-core multiconfiguration-Dirac–Hartree–Fock-adjusted pseudopotentials for post-d main group elements: Application to PbH and PbO, J. Chem. Phys. 113 (7) (2000) 2563–2569, https://doi.org/10.1063/1.1305880.
[37] K.L. Schuchardt, B.T. Didier, T. Elsethagen, L. Sun, V. Gurumoorthi, J. Chase, J. Li, T.L. Windus, Basis set exchange: a community database for computational sciences, J. Chem. Inf. Model. 47 (2007) 1045–1052, https://doi.org/10.1021/ci600510j.
[38] T. Lu, F. Chen, Multiwfn: a multifunctional wavefunction analyzer, J. Comput. Chem. 33 (2012) 580–592, https://doi.org/10.1002/jcc.22885.
[39] R. Hilal, S.G. Aziz, A.O. Alyoubi, S. Elroby, Quantum topology of the charge density of chemical bonds. QTAIM analysis of the C-Br and O-Br bonds, Procedia Comput. Sci. 51 (2015) 1872–1877, https://doi.org/10.1016/j.procs.2015.05.423.
[40] W. Wang, B. Ji, Y. Zhang, Chalcogen bond: a sister noncovalent bond to halogen bond, J. Phys. Chem. A 113 (2009) 8132–8135, https://doi.org/10.1021/jp904128b.
[41] R.F.W. Bader. Atoms in Molecules: A Quantum Theory, Clarendon, Oxford, U.K, 1990.
[42] C.S. López, A.R. de Lera, Bond ellipticity as a measure of electron delocalization in structure and reactivity, Curr. Org. Chem. 15 (20) (2011) 3576–3593, https://doi.org/10.2174/138527211797636228.
[43] T. L. Riss, R. A. Moravec, A. L. Niles, S. Duellman, H. A. Benink, T. J. Worzella, and L. Minor, Cell Viability Assays, In: Assay Guidance Manual, 2004, 1-25.
[44] P. Kumar, A. Nagarajan, P.D. Uchil. Analysis of Cell Viability by the MTT Assay, Cold Spring Harbor Protocols, 2018.